Computers and Electronics in Agriculture 160 (2019) 71–81

Contents lists available at ScienceDirect

Computers and Electronics in Agriculture

journal homepage: www.elsevier.com/locate/compag

Original papers

NU-Spidercam: A large-scale, cable-driven, integrated sensing and robotic system for advanced phenotyping, remote sensing, and agronomic research

Geng Bai[a], Yufeng Ge[a,*], David Scoby[b], Bryan Leavitt[c], Vincent Stoerger[d], Norbert Kirchgessner[e], Suat Irmak[a], George Graef[b], James Schnable[b,d], Tala Awada[c,f]

[a] Department of Biological Systems Engineering, University of Nebraska-Lincoln, Lincoln, NE 68583, USA
[b] Department of Agronomy & Horticulture, University of Nebraska-Lincoln, Lincoln, NE 68583, USA
[c] School of Natural Resources, University of Nebraska-Lincoln, Lincoln, NE 68583, USA
[d] Center for Plant Science Innovation, University of Nebraska-Lincoln, Lincoln, NE 68583, USA
[e] Institute of Agricultural Sciences, ETH Zurich, 8092 Zurich, Switzerland
[f] Agricultural Research Division, University of Nebraska-Lincoln, Lincoln, NE 68583, USA

ARTICLE INFO

Keywords:
Image analysis
Multispectral imagery
Thermal infrared imagery
LiDAR
Reflectance spectra

ABSTRACT

Field-based high throughput plant phenotyping has recently gained increased interest in the efforts to bridge the genotyping and phenotyping gap and accelerate plant breeding for crop improvement. In this paper, we introduce a large-scale, integrated robotic cable-driven sensing system developed at University of Nebraska for field phenotyping research. It is constructed to collect data from a 0.4 ha field. The system has a sensor payload of 30 kg and offers the flexibility to integrate user defined sensing modules. Currently it integrates a four-band multispectral camera, a thermal infrared camera, a 3D scanning LiDAR, and a portable visible near-infrared spectrometer for plant measurements. Software is designed and developed for instrument control, task planning, and motion control, which enables precise and flexible phenotypic data collection at the plot level. The system also includes a variable-rate subsurface drip irrigation to control water application rates, and an automated weather station to log environmental variables. The system has been in operation for the 2017 and 2018 growing seasons. We demonstrate that the system is reliable and robust, and that fully automated data collection is feasible. Sensor and image data are of high quality in comparison to the ground truth measurements, and capture various aspects of plant traits such as height, ground cover and spectral reflectance. We present two novel datasets enabled by the system, including a plot-level thermal infrared image time-series during a day, and the signal of solar induced chlorophyll fluorescence from canopy reflectance. It is anticipated that the availability of this automated phenotyping system will benefit research in field phenotyping, remote sensing, agronomy, and related disciplines.

1. Introduction

High throughput field-based plant phenotyping has recently attracted substantial interest because of its importance in: (1) closing the gap between plant genotyping and phenotyping, (2) accelerating the cycle of breeding for crop improvement, and (3) meeting the global demands of food, fiber and fuel that can be produced from agricultural sectors (Furbank and Tester, 2011; White et al., 2012). It is anticipated that appropriately deployed field phenotyping technologies will enable us the collection of high volume, multifaceted plant phenotypic data. These field measured data, together with the co-measured environmental variables, will enable an accelerated pace of scientific discovery, from understanding complex interactions between genotype and environment to identifying the best performers among thousands of candidate genotypes as part of crop improvement efforts (Araus and Cairns, 2013).

Field-based plant phenotyping platforms include manually operated carts (White and Conley, 2013; Bai et al., 2016), tractor-based vehicles (Andrade-Sanchez et al., 2014; Jiang et al., 2018) and field robotics (Underwood et al., 2017), and unmanned aerial vehicles (UAV) (Sankaran et al., 2015; Shi et al., 2016). Each platform has its own merits and limitations. For example, manually operated carts are light weight and flexible, but have lower measurement throughput and have difficulty scaling to the mature height of some crops (e.g., maize). Tractor-based platforms can be heavy and create undesired compaction in soil. Ground-based platforms could also cause mechanical damage to

* Corresponding author at: Department of Biological Systems Engineering, 203 Chase Hall, East Campus, University of Nebraska-Lincoln, Lincoln, NE 68583, USA.
E-mail address: yge2@unl.edu (Y. Ge).

https://doi.org/10.1016/j.compag.2019.03.009
Received 1 October 2018; Received in revised form 23 January 2019; Accepted 7 March 2019
Available online 16 March 2019

crops particularly in late growing season. UAVs, on the other hand, are suitable for tall crops, but have limited sensor payload capacity and measurement duration.

A fixed framework (such as a sensor platform supported by a gantry or cable-suspension system) over a large-sized field for high throughput plant phenotyping combines the merits of both vehicle-based and UAV-based platforms. It could easily measure tall crops and would not be limited by the sensor payload or battery capacity (meaning long measurement hours with multiple sensing modalities are possible). It would support measurements under the conditions of wet soil (not possible with vehicle-type) and mild to strong winds (not possible with UAV). Furthermore, the system can position and orient sensors to a particular plot with high accuracy and repeatability, which enhance the quality of field data for precision phenotyping.

Virlet et al. (2017) reported an overhead gantry system (Field Scanalyzer) for plant phenotyping research developed at Rothamsted Research, U.K. This system has a rectangular sensing area of 0.12 ha (116 × 11 m) and a height of 4.1 m. It has a sensor payload capacity of 500 kg. Sensors employed on this system comprise high-resolution visible, chlorophyll fluorescence and thermal infrared cameras, two hyperspectral imagers and dual 3D laser scanners. However, it was highlighted in this publication that processing of images from hyperspectral imagers and laser scanners was still challenging. Kirchgessner et al. (2017) reported a cable-suspended field phenotyping system at ETH Zurich. It covered 1 ha of experimental field with a maximum sensor height of 6 m. The control system could be programmed to move the sensor platform to locations by inputting XYZ coordinates. The system was more compact and the cables minimized the shadow problem that could bias the measurement and increase the complexity of image processing. The authors demonstrated the use of multiple sensor modules to measure various crop traits, including ground cover, plant height, canopy temperature and spectral reflectance.

In this paper, we reported a large-scale, cable-driven, integrated sensing and robotic platform for high-precision, field-based plant phenotyping research developed at University of Nebraska, U.S. (NU-Spidercam). We described the design and development of the system in terms of: (1) hardware integration of various imaging, ranging and spectroscopic sensors, and (2) software development for task planning, motion control, and automated measurements. The system was tested in 2017 and 2018 growing season. We also reported the system performance and provided examples of novel phenotypic data enabled by the system.

2. Design and development of NU-Spidercam facility

2.1. Facility overview

The NU-Spidercam facility is located at Eastern Nebraska Research and Extension Center of the University of Nebraska, Mead, NE, U.S. (41°08′44.4″ N, 96°26′20.6″ W, 369 m above sea level). The field is approximately 2.0 ha, with a core imaging area of ~ 0.4 ha (60 × 67 m, Fig. 1A and B). The two soil types are Yutan silty clay loam and Filbert silt loam. The core imaging area is divided into 128 zones. Each zone is 4.6 × 6.1 m (Fig. 1B) and contains six crop rows with a row spacing of 0.76 m. A variable-rate, subsurface drip irrigation (SDI) system was installed 0.25 m below the surface, which can apply different amounts of irrigation water to each zone (Fig. 1C). A two-story observation and control building was built on the site to house main electric, electronic, communication, monitoring and control devices for the facility (Fig. 1D).

The sensor platform (Fig. 1E) is suspended and driven by eight Kelvar cables from four poles at the corners of the core imaging area. The cables are pulled by four winches to position the sensor platform in the imaging area via a proprietary algorithm (Spidercam GmbH, Austria). The positioning accuracy is ± 5 cm in XYZ directions. The poles are 27 m high; and the designed height range of the sensor platform is 0–9 m (from the ground). This allows researchers to collect phenotypic data on tall crops such as maize and biomass sorghum throughout the growing season. The sensor platform can move at a maximum speed of 2 m/s. This means it can move between any two plots in the imaging area within 45 s. The sensor platform has a payload capacity of 30 kg (in addition to the mass of the battery and the controlling computer). Other major components that support the operation of the facility include an SDI control room, an electric building, and four winch houses where the winches are operated. Fig. 1 provides an overview of the NU-Spidercam facility, the field layout, and its major components.

2.2. Integration of plant sensors onto the sensor platform

A number of plant sensors are integrated on the sensor platform to capture multi-modal plant traits. The plant sensors include a four-band RGB-NIR (multispectral) camera, a thermal IR camera, a 3D scanning LiDAR, and a VNIR portable spectrometer. A fanless embedded computer (NDiS B535, Nexcom) which controls all sensor modules, takes sensor readings, and stores the measurements is integrated into the sensor platform. Table 1 provides detailed information regarding the sensors, their connection and communication with the computer, and the plant parameters measured.

The portable VNIR spectrometer is connected to two optical fibers via a bifurcated optical fiber and two electronic shutters (INLINE-TTL, OceanOptics). One optical fiber is aimed down to measure reflected solar energy from crop canopy (upwelling), and the other fiber (to which a cosine corrector is attached) is pointed to the sky to measure incoming solar irradiance (downwelling). The shutters are triggered by TTL (Transistor-Transistor-Logic) signals from the computer to activate the two optical fibers sequentially. Each measurement therefore is consisted of two sets of spectrometer readings: one set corresponding to when the upwelling (again looking at the surface) fiber is activated and the other set the downwelling (again looking at the sky) fiber activated. This dual optical fiber design effectively accounts for varying sky condition due to solar elevation and clouds and allows accurate measurements of crop canopy reflectance.

The RGB-NIR camera, thermal IR camera, LiDAR and upwelling optical fiber are mounted on a pan/tilt unit at the bottom of the sensor platform (Fig. 2A). They are placed such that they share a common field of view on the ground, which ensures the measurements from different sensors cover the same area and can be related. Fig. 2B illustrates the field of view of each sensor when the sensor platform is approximately 5 m above the ground (or canopy). Although all measurements reported in this paper were from a nadir view, the pan/tilt unit does allow the sensors and cameras to take measurements at slanted angles (Supplemental Fig. 1), which can be of great value for multi-angle imaging and remote sensing research.

An anemometer, a GPS receiver, and the downwelling optical fiber are mounted on the upper part of the sensor platform (Fig. 3). GPS was currently not used for positioning, because NU-Spidercam itself has a positioning system that is more precise. The controlling computer, spectrometer, batteries, and all supporting components (such as Ethernet cable switches, wires, voltage converter, etc.) are also mounted on the upper part of the platform and are protected by a cover from rain and direct sun light during operation.

The sensor platform is powered by two batteries supplying unregulated 48 VDC. A power conversion block is used to convert 48 V to regulated 12 and 24 V to power the computer and various sensor modules (Table 1). When fully charged, the battery can support 6–8 h of operation.

2.3. Software development

The program for the sensor platform task planning, motion control and data collection was developed using LabVIEW (Version 2016, National Instruments, Austin, Texas, U.S.). Fig. 4 shows the

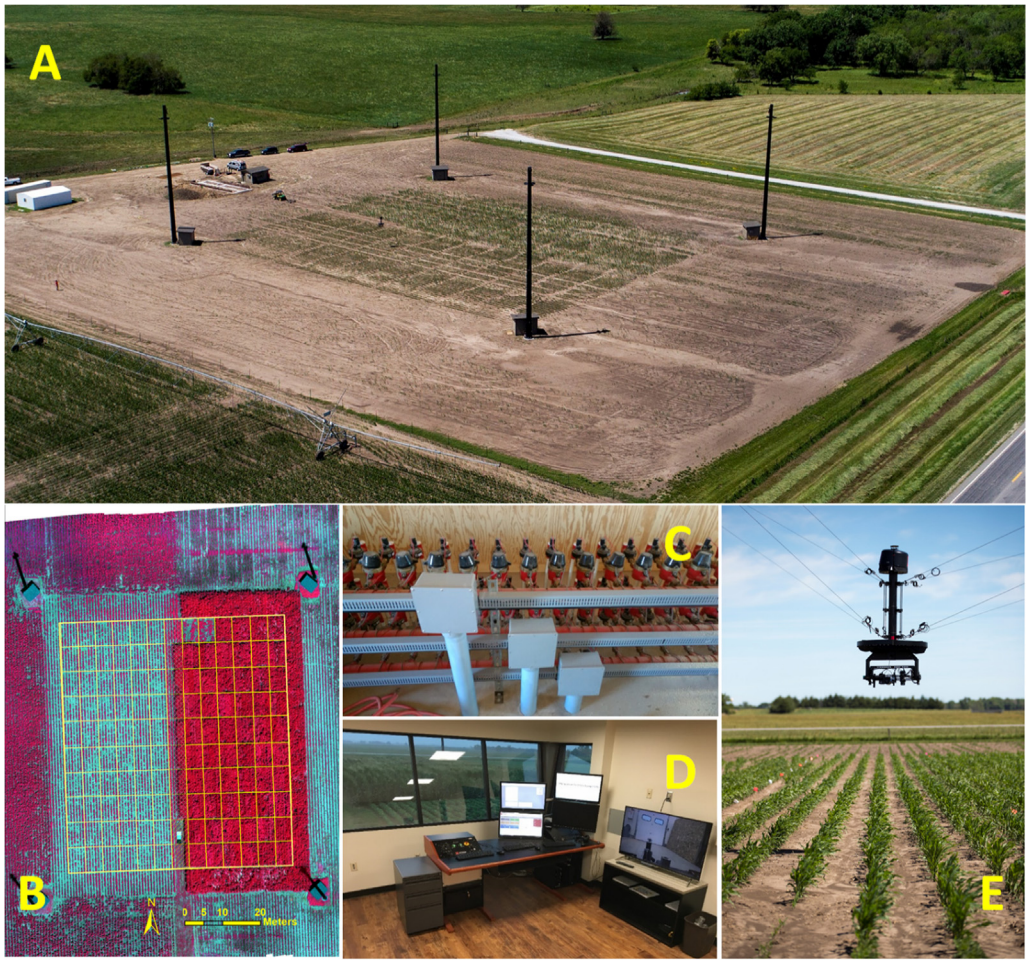

Fig. 1. NU-Spidercam field phenotyping facility. A – Bird view of the facility; B – the 128 zones in the core imaging area; C – the control valves of the variable-rate subsurface drip irrigation system; D – the control and observation building; E – a close-up view of the sensor platform.

Table 1
Plant sensors onboard NU-Spidercam's sensor platform.

Sensor	Description	Connection, power, and driver	Parameters
Multispectral camera	AD080GE, JAI Spectral window: 400–650 nm (RGB) and 760–1000 nm (NIR) Resolution: 1024x768 pixel Field of View: 44.9° (H) and 34.0° (V)	Ethernet 12 VDC LabVIEW IMAQdx	Vegetation coverage Soil fraction Canopy NDVI Soil NDVI
Thermal IR camera	A655sc, FLIR Spectral window: 7.5–14 μm Resolution: 640x480 pixel Field of View: 24.8° (H) and 18.8° (V)	Ethernet 12 VDC LabVIEW IMAQdx	Canopy temperature Soil temperature
Spectrometer	HR2000+, OceanOptics Spectral window: 450–880 nm; spectral sampling: 1/5 nm Field of View: 25°	USB Powered also by USB OceanOptics LabVIEW Driver	Canopy reflectance spectra Vegetation indices
3D LiDAR	VLP-16 Puck, Velodyne Field of view: ± 15° cross track	UDP via Ethernet 12 VDC No special driver needed	Canopy height

initialization Graphic User Interface (GUI) of the program. During initialization, the program checks the current status of the sensor platform and ensures it is ready for motion. Sensor modules can be individually selected or de-selected to meet the need of each measurement campaign. The option of "hyperspectral camera" is reserved for future integration.

For task planning, researchers upload a 'Way-Point Map', which is a TXT file with a set of predefined locations (for example, the center of each zone or plot) in the core imaging area. Each line of the TXT file contains the XYZ coordinates of a location and Pan/Tilt angles of sensor orientation, and a desired driving speed for the sensor platform (Supplemental Fig. 2). The program will also check to ensure the locations are in acceptable ranges, and display them in "Graph Display of Map File" of the GUI (Fig. 4A). The program then generates a custom XML-based command for each line of the TXT file (Supplemental Fig. 3), and sends them sequentially to a computer that is dedicated for winch control and cable feeding.

There are two modes of motion control for the sensor platform in

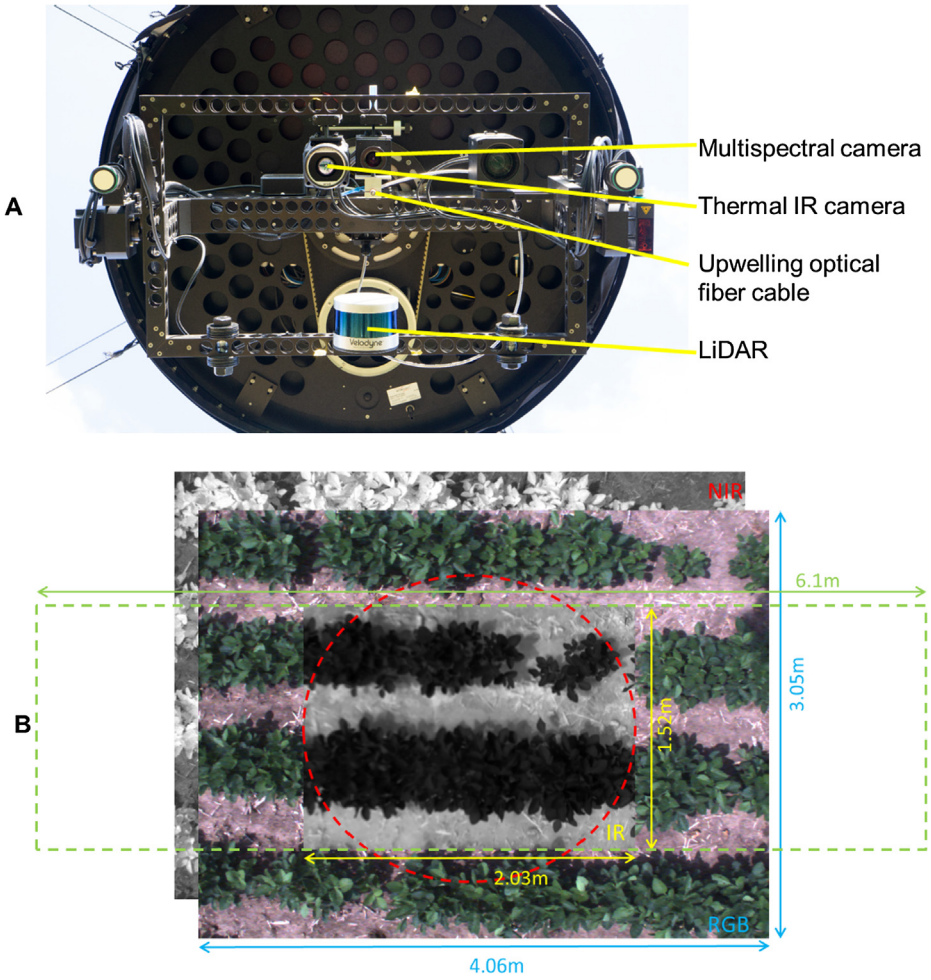

Fig. 2. A – The physical layout of the plant sensors at the bottom of the sensor platform; B – Field of view of the multispectral camera, thermal IR camera, upwelling optical fiber cable (red dashed line circle) and LiDAR scanning swath (green dashed line rectangular area). (For interpretation of the references to colour in this figure legend, the reader is referred to the web version of this article.)

the program. The first one is “stop-measure-go”. In this mode, the sensor platform is driven to a location, stopped to stabilize and take measurements, and then driven to the next location. Because the platform is operated only a few meters above crop canopy, this pattern ensures best image quality with minimum image blurring caused by the relative motion between the imaging sensors and plants. The second mode is “continuous”, where the sensor platform traverses through target locations without stopping. The program uses a separate control loop to trigger the sensors continuously. In this mode, images are captured with significant overlap that allow the mosaic of the entire imaging area (similar to UAV imaging). This mode is also necessary for push-broom type hyperspectral imaging system. Fig. 5 provides a high-level flow chart diagram for automated measurement using the “stop-measure-go” mode.

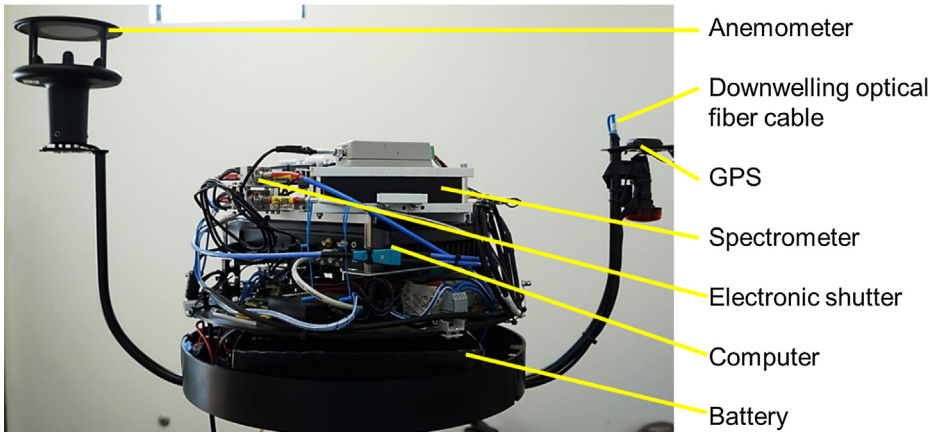

Fig. 3. Upper part of the sensor platform with the anemometer, downwelling optical fiber cable, GPS, spectrometer, electronic shutters, computer, battery, and other supporting electronics.

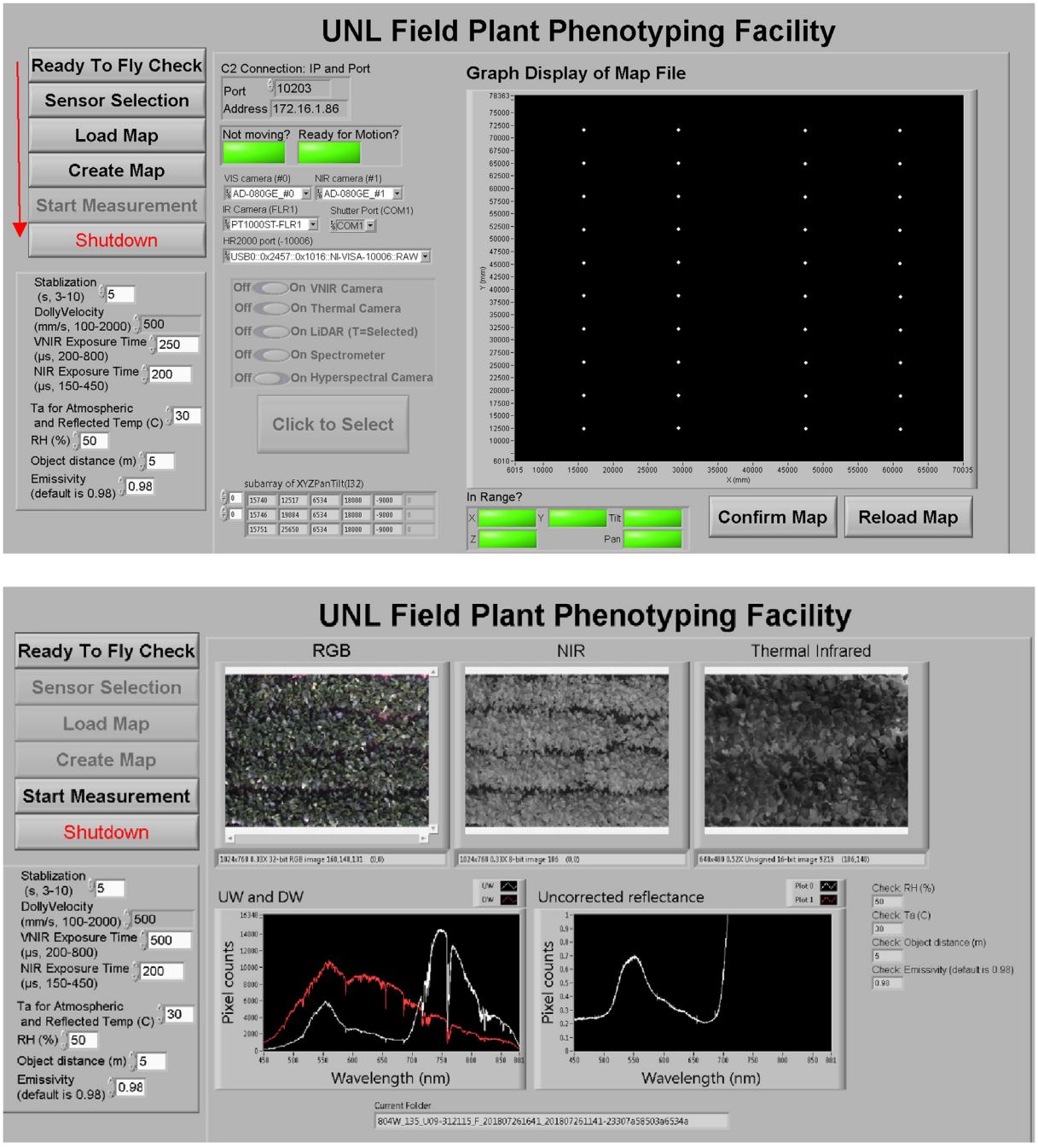

Fig. 4. Graphic User Interface (GUI) of the NU-Spidercam program developed with LabVIEW: (A) the initialization page for sensor selection and mission planning; and (B) the measurement page providing real time update of sensor data and images being captured.

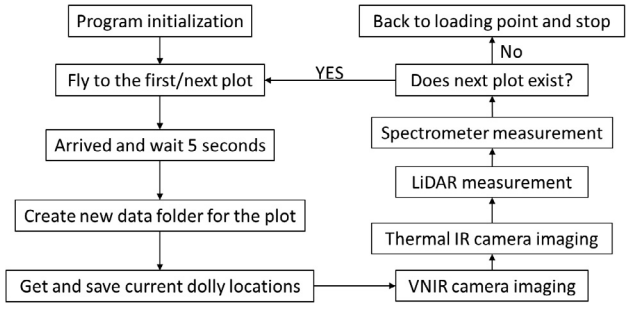

Fig. 5. High-level flow chart diagram for automated measurement using the "stop-measure-go" mode.

The program provides a live update of the multispectral image, thermal IR image, and downwelling and upwelling spectra of the current plot being measured (Fig. 4B).

Measurement data and experimental metadata are stored in the controlling computer with a two-level file directory system. At the first level, data are organized by "Date". Within a "Date" folder, measurements from each location is stored in a subfolder (second level) and the subfolder name is "Location ID_Serpentine number_Genotype_Irrigation level_Time stamp_XYZ". In this manner each measurement is unambiguously linked to a location (or plot) and measurement time. Inside the second level folders, measurement data including the multispectral image, thermal IR image, spectral data, and LiDAR point cloud are saved. The metadata including the XYZ coordinates, pan-tilt angles, and speed of the sensor platform are also saved in the folder.

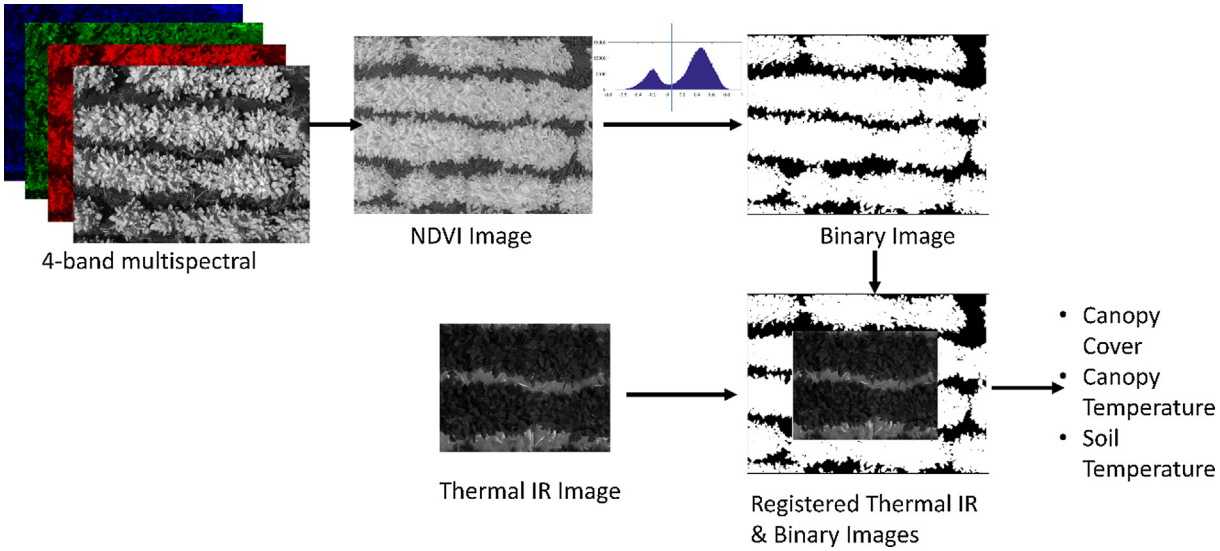

Fig. 6. Joint analysis of multispectral image and thermal IR image to extract plot-level canopy cover, canopy temperature, and soil temperature.

2.4. Variable rate SDI and onsite weather station

The variable rate SDI for the NU-Spidercam facility is unique in the sense that it controls the 128 zones (Fig. 1B and C) which can be irrigated and fertigated independently with high water application uniformity (Christiansen Uniformity Coefficient of > 98%). Water can be applied with a precision of 0.04 L each zone, enabled by state-of-the-art pressure compensating emitters which compensate changes in operating pressure and provide constant (and targeted) flow rate. The irrigation events can be automatically triggered based on predetermined soil moisture threshold in the crop root zone or crop water use. This level of precision, uniformity, and automation with the SDI is highly desirable for studying plant traits related to irrigation response, stomatal conductance, water use, and nitrogen use.

An automated weather station was emplaced approximately 30 m west of the NU-Spidercam facility. The weather station collects weather and environmental parameters, including air temperature (Ta) and relative humidity (2 m above the ground), precipitation, wind speed and direction (3 m above the ground), photosynthetically active radiation (PAR), and total shortwave radiation. These variables are recorded at one minute interval. These data are used together with plant measurements from NU-Spidercam to help elucidate the interaction between genotypes and environment.

3. Field experiment to test the NU-Spidercam facility

The NU-Spidercam facility was tested for two years during the 2017 and 2018 growing season. In 2017, soybean with different genotypes was planted on the east half of the field while maize was planted on the west half of the field. The 180 two-row maize plots included 162 maize hybrids constructed from crossing maize inbreds developed by major seed companies and released following the expiration of plant variety patents, plus a repeated modern check line. The expired plant variety patent maize hybrids were selected to match those being grown and phenotyped at several dozen locations across the U.S. and Canada as part of the Genomes to Fields project (Gage et al., 2017). The experiment in 2018 was similar, except that soybean was planted on the west half and maize on the east half to mimic a maize-soybean rotation commonly employed in the region.

In 2017, the sensor platform was operated at 9 m above the ground. At this height, the multispectral camera covered 10 rows of crop and thermal IR camera covered 6 rows. In 2018, the sensor platform was operated at 5 m above the ground. At this height, the multispectral camera covered 4 rows of crop and thermal IR camera covered 2 rows. Primary motion control mode was “stop-measure-go”. Continuous motion mode was conducted a number of times to evaluate the performance of image mosaicking like UAV.

The purposes of the experiment were three fold. Firstly, we evaluated the functionalities and robustness of hardware and software components of the system during actual field operations. Secondly, we validated the sensor measurements with the ground truth measurements. In particular, we validated the LiDAR measurements against manual measurement (using a yardstick) of plot heights, and crop thermal IR images against canopy temperature measured by a handheld IR radiometer (Omega Engineering, Norwalk, Connecticut, U.S.). More information regarding ground truth measurement is in Supplemental Fig. 4. Thirdly, we demonstrated the usefulness of the facility for high-precision plant phenotyping research by collecting relevant plot-level plant trait data from genotypes for which extensive conventional field phenotyping data exists.

We extracted crop coverage from four-band RGB-NIR multispectral images. An NDVI image was calculated using NIR and R bands of the image: (NIR-R)/(NIR + R). The NDVI image was effective to segment crop pixels from soil background by setting a single threshold. Crop coverage was calculated as the number of crop pixels divided by the total number of pixels.

An affine transformation was developed that allowed the overlay of the thermal IR image to the RGB-NIR image. Because the relative position of the thermal camera and the multispectral camera was fixed, one affine transformation could apply to all the image sets captured by the system. After the overlay, we used the binary image (derived from the NDVI image) as a mask to segment the thermal IR image into crop and soil fractions. This procedure was more accurate than a direct segmentation of the thermal IR image using an automatic threshold method (such as Otsu method). Average crop canopy temperature (Tc) was calculated by averaging the temperature of all plant pixels. Similarly, average soil temperature (Ts) was calculated by averaging the temperature of all soil pixels (Fig. 6).

Crop height at the plot level was extracted from LiDAR data. Raw LiDAR points were filtered to remove points that fell outside the targeted plot. The distance between the soil and the LiDAR sensor (D1) was determined using data from the earliest date of the year (when soil exposure was the greatest) and the maximum distance (or 100 percentile) was used. The distance between plot canopy and the LiDAR sensor (D2) was determined using the 10 percentile distance of the filtered LiDAR points. Average canopy height was then calculated by

subtracting D2 from D1. Note this method assumed D1 was constant over the time. This assumption was realistic because the sensor platform could be driven to the same location with high precision.

Eq. (1) was used to convert the raw spectral readings to canopy reflectance.

$$R(\lambda) = CF(\lambda) \times \frac{DN_{UW}(\lambda) - Dark_{UW}}{DN_{DW}(\lambda) - Dark_{DW}} \quad (1)$$

where R is canopy reflectance. DN_{UW} is the digital number output of the spectrometer when the upwelling fiber is activated. DN_{DW} is the digital number output of the spectrometer when the downwelling fiber is activated. $Dark_{UW}$ and $Dark_{DW}$ are the dark pixel values measured by closing the shutters after the upwelling and downwelling measurements. λ indicates the variables are wavelength dependent. CF is the correction factor (also wavelength dependent), which is derived by scanning three reflectance tarps of known spectral reflectance. The tarps are 1.62 × 1.62 m in dimension (nominal reflectance values of 5, 45, and 75%) and set up inside the imaging area during the operation for spectral calibration (Supplemental Fig. 5).

4. Results and discussion

4.1. Functionality and robustness of NU-Spidercam

In 2017, operations were carried out on 13 days between 7/12 and 9/28. Each day the system was run 5–6 h on average. There were two problems in 2017. Firstly, the motion control and sensor trigger part of the program were not well integrated, and in several occasions, the sensor platform was driven to measurement locations manually via a joystick. Secondly, frequent exceptions occurred for one winch that fed the Kelvar cables. Both problems reduced the measurement throughput significantly and were addressed after 2017 growing season.

In 2018, operations were carried out on 20 days between 7/9 and 9/14. In most of these days, the system was set to take plot-level measurement with full automation (without operator's intervention). All desired functions of the system regarding task planning, motion control, and automated data collection were realized. The system also exhibited outstanding robustness in the weather conditions of no rain nor strong wind ($> 10\,m\,s^{-1}$). For most days, the system was run continuously without hardware or software errors. It took ~4 h to cover the entire 360 two-row plots with the "stop-measure-go" mode. Note that this measurement throughput can be improved by: (1) increasing the moving speed of the sensor platform, and (2) shortening the waiting time to allow the sensor platform to stabilize. It is feasible to go over the entire field twice (720 two-row plots) in a day. A time-lapse video showing the operation of NU-Spidercam in a typical day is provided in the Supplemental Material.

4.2. Quality of sensor data in comparison to ground truth data

Fig. 7 compares crop canopy temperature and height measured by the sensor platform vs. the ground truth measurements in selected soybean plots. For canopy temperature, the two sets exhibited strong linear correlation (R^2 = 0.931). Root mean squared error (RMSE) was 1.84 °C. The temperature measured by the sensor platform was consistently higher, as indicated by a unity slope but non-zero intercept of 1.67 °C. Because the thermal IR camera and the handheld IR radiometer were not cross-calibrated, this systematic bias could be due to the discrepancy in calibration between the two devices. Another factor that would introduce random error was the fact that the thermal IR camera and the IR radiometer measured the same canopy at slightly different time (roughly two minutes difference). Canopy temperature is a dynamic trait that can change rapidly in a short time, especially under varying clouds and intermittent winds. This random error therefore could indicate the real canopy temperature differences measured at slightly different times.

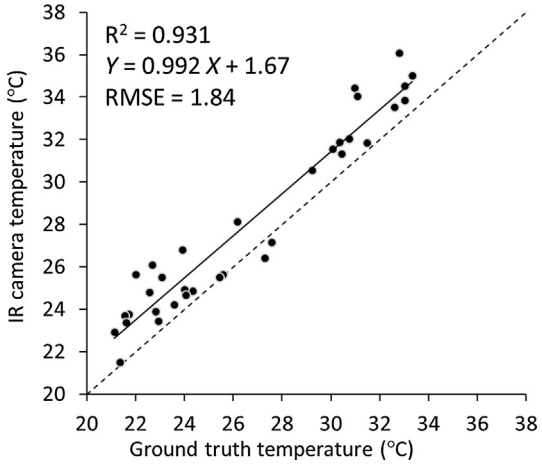

Fig. 7. Validation of canopy temperature measured from the NU-Spidercam sensor platform against the ground truth measurements.

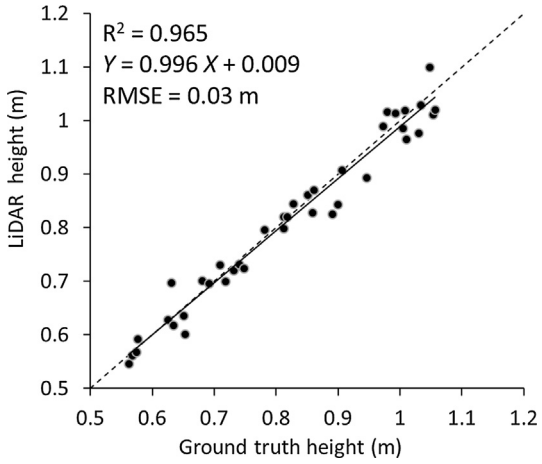

Fig. 8. Validation of the canopy height measured from the NU-Spidercam sensor platform against the ground truth measurements.

Canopy height measured by the LiDAR and yardstick exhibited strong linear correlation (R^2 = 0.965) and RMSE was 0.03 m in selected soybean plots (Fig. 8). The slope of the regression line was close to 1 and the intercept was close to 0, indicating LiDAR measurements were not biased. With this ground truth validation, LiDAR appeared be a reliable method for canopy height measurements. This level of performance was also consistent with other studies that used LiDAR as a high throughput tool for plant height measurements (Madec et al., 2017; Jimenez-Berni et al., 2018).

4.3. Examples of measurement data enabled by NU-Spidercam

Fig. 9 shows canopy height and vegetation cover of the soybean crop (180 plots) in 2018 between Jul/10 and Aug/15. The average height increased steadily from 0.4 m to over 1.0 m on 8/10. On 8/15 overall height decreased slightly. This is because a portion of the plots started to lodge when entering late reproductive stage. Average canopy cover also showed a steady increase from ~35% to 80% on 7/26. Thereafter, the increase slowed down and average canopy cover approached ~100% around 8/07. This kind of information is desirable for high throughput phenotyping platform, because it allows the measurement of key growth parameters multiple times along the growing season. Further processing can be done to fit the functional growth curves and analyze growth patterns.

Although the stop-measure-go motion mode was predominantly

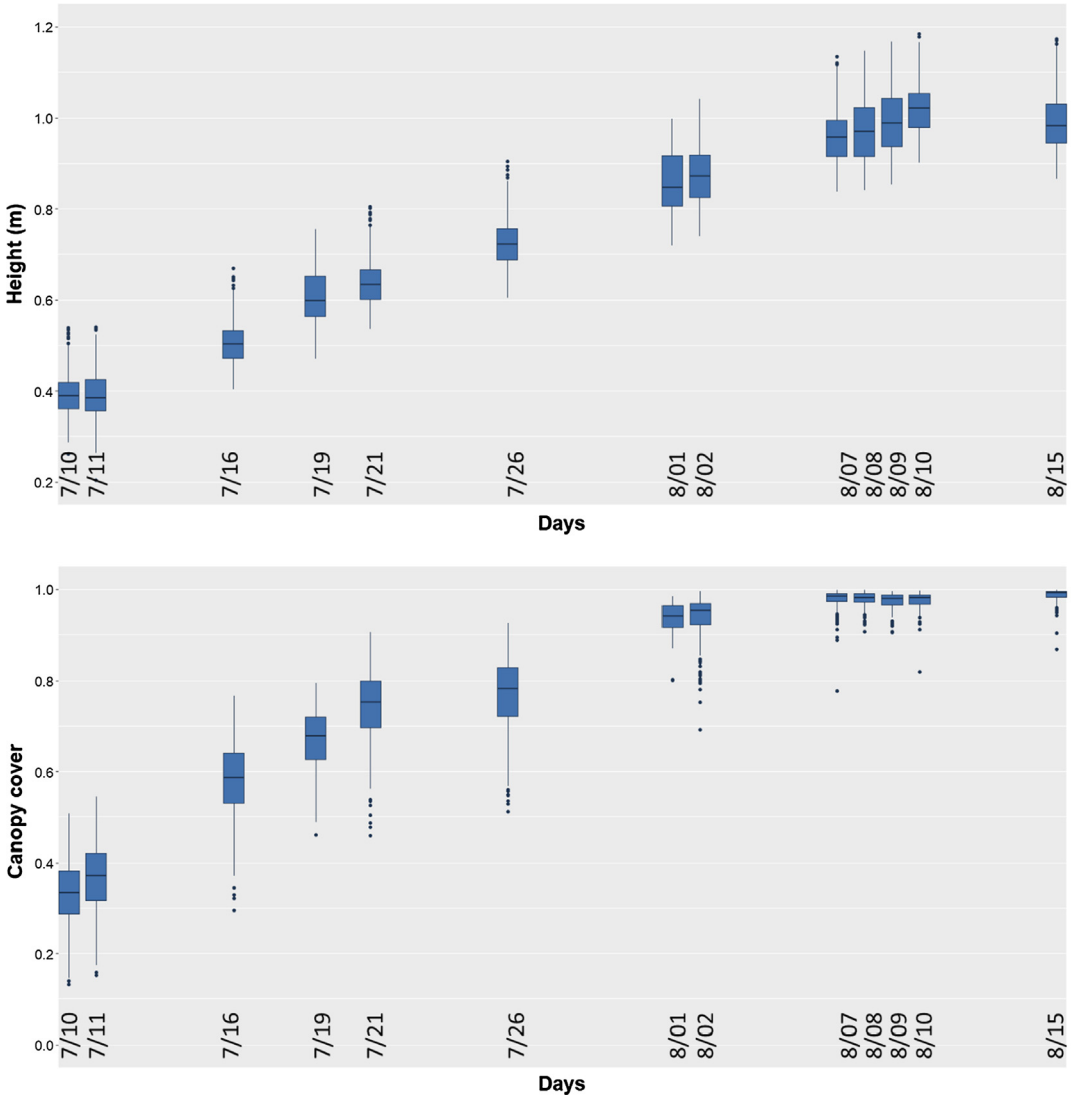

Fig. 9. Time series of plant height (extracted from LiDAR) and canopy cover (extracted from multispectral images) of soybean (180 two-row plots) in 2018.

Fig. 10. Mosaicked RGB images of plant canopies from the continuous motion mode of NU-Spidercam A: The soybean canopy image mosaicked automatically with Pix4D; B: The maize canopy image mosaicked manually with Photoshop.

used, we did collect images with continuous motion mode to demonstrate the feasibility of image mosaicking similar to UAV. The sensor platform was driven from the left side of Fig. 10A to the right side with a constant speed of 0.5 m/s. The multispectral camera was set to capture images at 0.25 s interval. The two consecutive images had an offset of 0.125 m, equivalent to a ~96% image overlap. There was a total of 214 images in this pass (covering 18 2-row soybean plots), and they were successfully mosaicked using Pix4D software (Lausanne, Switzerland). Contrasting canopy characteristics caused by the different maturation in the soybean genotypes (again in 2-row plots) can be clearly identified in Fig. 10A. In addition, we also derived a maize canopy image (Fig. 10B) with the same imaging setting but the images were mosaicked manually using the photo merge function in Photoshop. Similarly, large phenotypic variation among the maize genotypes can be clearly seen from the mosaicked image.

NU-Spidercam enables us to collect plant data that are not easy to obtain with other phenotyping platforms. For instance, Fig. 11 shows the thermal IR images (pseudo color-coded to enhance contrast) of a two-row soybean plot (imaged repeatedly 12 times in a day between 12:00 and 6:00 PM local time). This time-series images shows a number of interesting patterns regarding the temperature dynamics of crop canopy versus soil. First, soil exhibited higher temperature than crop canopy. Second, at some time points the canopy had a more uniform temperature distribution (e.g., T2 and T3 in Fig. 11) while other times it was quite heterogeneous. Sun lit part of the canopy had higher temperature than the shaded part.

We further processed the time-series thermal IR images to segment crop from soil and extracted the average temperatures of crop vs. soil. In addition, we also extracted air temperature and PAR radiation from the weather station at the time when each plot was measured. Fig. 12 shows the result from this analysis for all 36 plots we tracked that day (7/19/2018). It can be seen that temperature of crop and soil increased

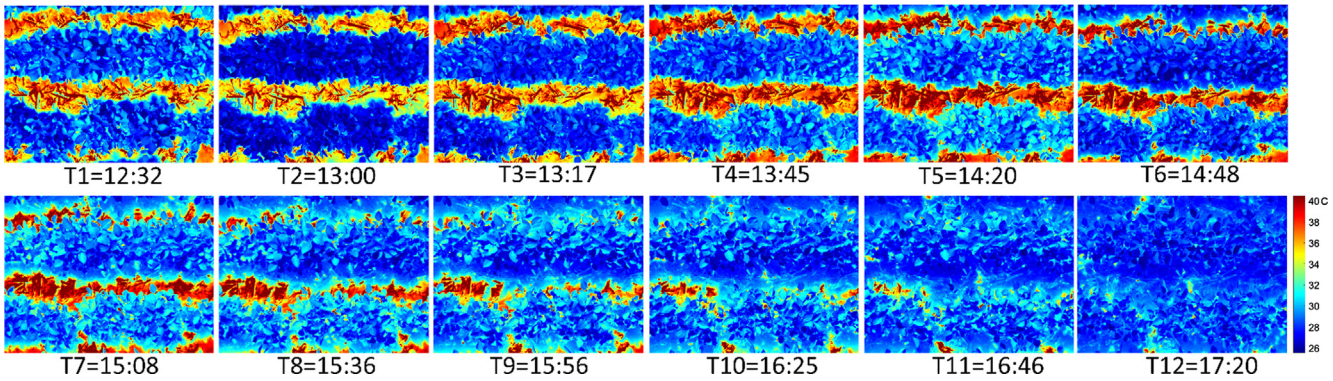

Fig. 11. Visualization of thermal IR image time-series of a soybean plot captured during a day.

and peaked at ~3:00 and ~2:00 PM respectively local time, and then decreased in late afternoon. The maximum temperature difference of soil vs. crop was about 8.35 °C at 13:38PM. Interestingly, air temperature continued to rise till the end of measurement (~5:30 PM). The local solar noon was around 1:30 PM; which coincided with peak PAR. There was large variation of canopy and soil temperature among the different plots (scatters around the fitting line). This is likely caused by genetic factor and the differences in vegetation cover among the plots.

Figs. 11 and 12 revealed complex spatial and temporal patterns of crop canopy vs. soil temperature within a day. To the best of our knowledge, this type of information has not been reported in the literature. Although thermal imaging is common in satellite and aerial remote sensing, thermal images from these platforms are coarse in spatial resolution and not able to provide this level of spatial granularity. Capturing the temporal dynamics of canopy temperature for different plots as shown in Fig. 12 is even more challenging for the conventional phenotyping platforms including UAVs and ground-based phenocarts, as it may not be practical to go over the field multiple times in a day using these platforms.

Canopy temperature is a critical variable and is widely used to relate leaf stomatal conductance or water stress (Li et al., 2014) and for determining the irrigation timing and yield vs. crop water stress relationships (Irmak et al., 2000; Payero and Irmak, 2006). Non-imaging infrared radiometers are often employed in the field for this purpose. One of the potential problems with the non-imaging sensor is the mix of canopy and soil within sensor's field of view, which would bias the measurement. Furthermore, the degree of bias depends on: (1) the percent of vegetation cover and (2) the time of measurement during a day. It would be challenging to decouple these two confounding factors for the non-imaging sensor. Another important challenge with using non-imaging infrared thermometers is that multiple measurements from E-W and N-S directions must be taken into account for sun angle impact on canopy temperature, which also requires additional time. Since the measurements are taken directly above the crop canopy with the Spidercam thermal IR imagery, this challenge is minimized. Therefore, we expect this type of measurements from NU-Spidercam will allow us to better utilize thermal IR images as a tool for drought and water use related phenotyping.

Fig. 13 shows canopy reflectance of selected soybean and maize plots at 7/21, 7/26, 8/10, and 9/11 in 2018 with corresponding RGB images. The RGB images below the spectral reflectance figures indicate the canopy development in the FOV of the spectral measurement. The increase of the spectral reflectance in NIR was found in the soybean plot until 8/10, clearly due to the canopy development. Soybean leaves started yellowing on 9/11 and the reflectance at the NIR region decreased. For the maize plot, canopy growth was not noticeable from RGB images and the tassels were already established on 7/21. On 9/11, most of the maize plant leaves were yellow with few green leaves left. The spectral reflectance showed distinctive pattern comparing to that from green vegetation.

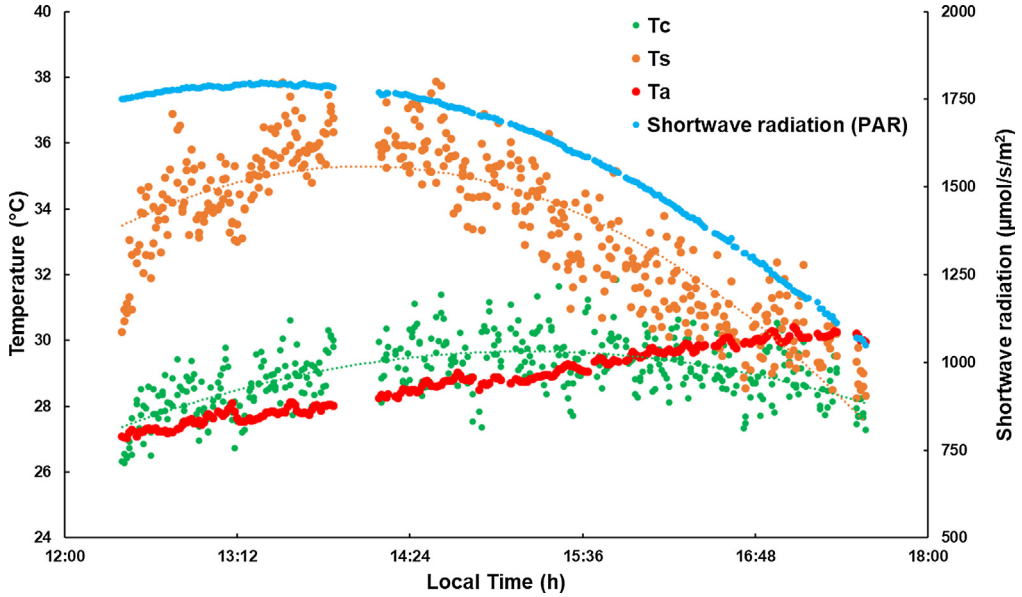

Fig. 12. Temporal dynamics of plot-level canopy temperature (Tc) and soil temperature (Ts) in contrast to air temperature (Ta) and photosynthetically active radiation (PAR).

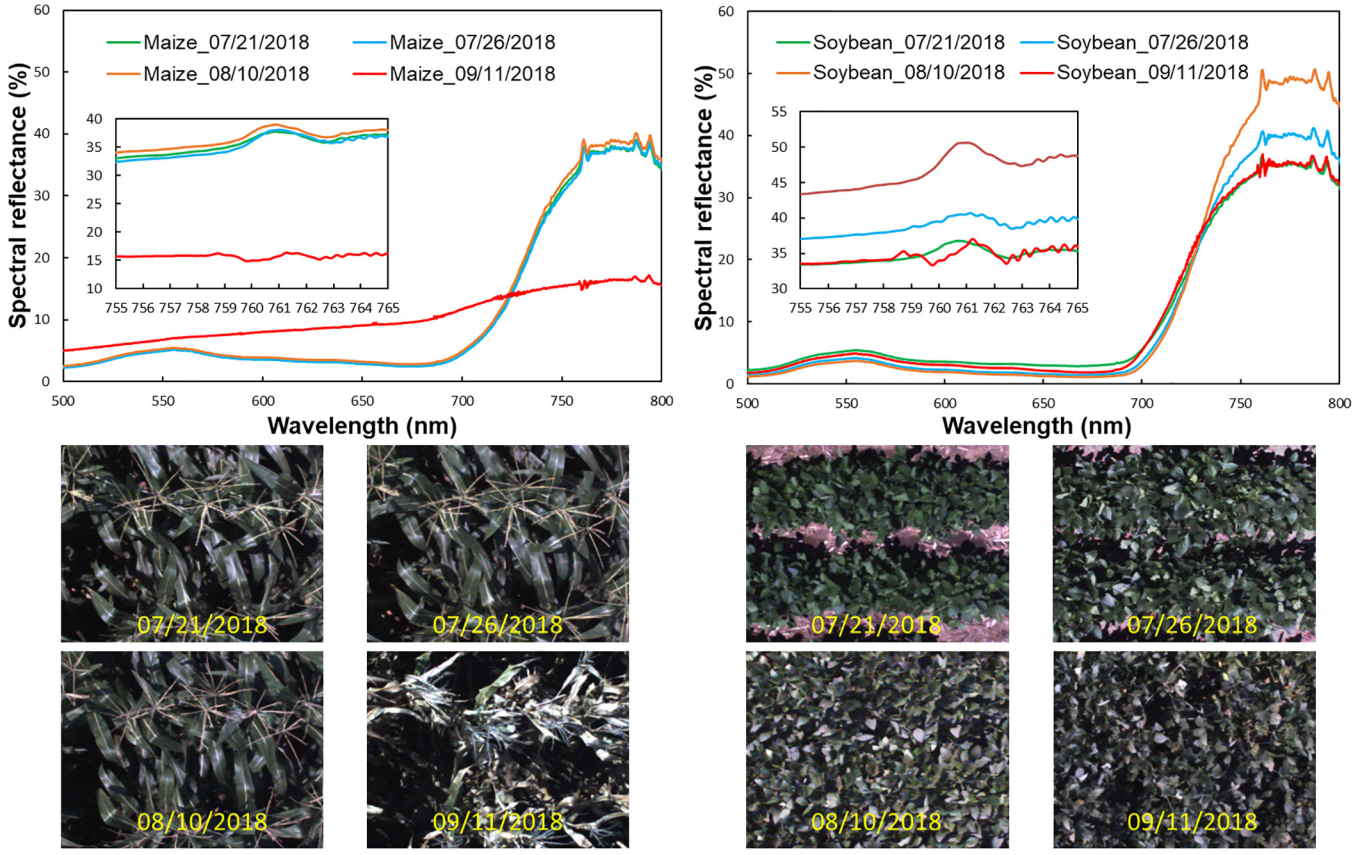

Fig. 13. Spectral reflectance of the selected soybean and maize plot on 7/21, 7/26, 8/10 and 9/11. The insets are the reflectance around the O_2-A band (760 nm) showing potential of retrieving solar induced chlorophyll fluorescence (SIF) signals from spectral data.

From the spectral data, we could calculate a number of vegetation indices from the canopy reflectance spectra in the future study, including NDVI (Normalized Difference Vegetation Index), NDRE (Normalized Difference Red Edge Index), PRI (Photochemical Reflectance Index), and CCI (Canopy Chlorophyll Index). These vegetation indices are commonly used as proxies to infer structural and biochemical properties of crops in both remote sensing and field phenotyping.

One application with great potential of the spectral data from our NU-Spidercam system is the measurement of solar induced fluorescence (SIF) signals from chlorophyll. SIF could be manifested as a small bump riding on the reflectance signal at ~760 nm (O_2-A band) (Meroni et al., 2009). 'Spectral bump' near 760 nm could be observed in the insets of Fig. 13. For the spectral reflectance of the corn plot on 9/11, 'spectral bump' disappeared as there was low leaf chlorophyll content for senescent maize. SIF has been reported in the remote sensing literature for broad-scale vegetation monitoring (Guanter et al., 2014), and shown to be correlated with photosynthesis and primary productivity (Sun et al., 2017). Radiometric calibration has not been carried out in this study but we will work on the retrieval of SIF signals from the spectral measurement which might lead to novel means of SIF for plant phenotyping research.

4.4. Future development

Although the NU-Spidercam has been successfully developed and tested, there are still many aspects regarding hardware, software, and operation that need to be improved. In the near term, we will incorporate a push-broom hyperspectral camera into the sensor platform and develop a continuous motion mode suitable for hyperspectral image acquisition along with all other sensor modules. We will also look into the control of the pan/tilt unit of the sensor platform which will make non-nadir measurement (i.e., multi-angle imaging) possible. In the long run, we also aim at developing a data infrastructure that will store the phenotyping data into a database and send the data into University of Nebraska's High Performance Computing Center in a real time fashion.

5. Concluding remarks

NU-Spidercam is one of three key investments in advanced phenotyping infrastructure at the University of Nebraska for phenotyping and transformational plant biology research. The other two systems are a Lab Scanalyzer HTS (LemnaTec GmbH) for Arabidopsis and a Greenhouse Scanalyzer for plants of agriculture importance (maize, sorghum, soybean, etc., Ge et al., 2016; Pandey et al., 2017; Liang et al, 2018). It is envisioned that these three research facilities will complement and amplify each other for plant genomics-phenomics discovery pipelines. Forward phenomics can be performed where potential new genotypes can first be fully characterized in the lab or greenhouse and then tested under NU-Spidercam for their field relevance. Alternatively, backward phenomics can be performed where a large number of candidate genotypes can go to the field first, and a few lines exhibiting superiority in targeted traits can be imaged in greater details in the lab or greenhouse to dissect their genetic basis. In either case, NU-Spidercam will play a critical role to provide high precision field phenotyping and relevant environmental data for the transformational plant biology research.

Although NU-Spidercam has a number of advantages (such as large instrument payload, high measurement resolution and flexibility, and less weather dependent), it is capital-intensive. The cost for developing such a facility is high and may not be affordable to individual research

group. On the other hand, technologies like UAVs and phenocarts are low in deployment cost and widely adopted in field phenotyping research. The intention of NU-Spidercam is not to replace other field phenotyping devices such as phenocarts or UAVs. Rather, these systems can work synergistically to increase the overall efficiency of plant phenotyping and the overall rate of trait discovery. NU-Spidercam is flexible and can position the sensor platform over crop plots precisely. Phenotyping data from NU-Spidercam is therefore of better quality and with greater spatial and temporal resolution. Knowledge gained from NU-Spidercam can inform the implementation of other phenotyping systems. For example, high quality hyperspectral imagery can be obtained with NU-Spidercam to determine the best three or four spectral bands to measure certain traits (e.g., chlorophyll content or water content) of a crop. Then a lower-cost, light weight multispectral camera dedicated to image those bands can be developed and launched on UAVs to measure these traits in different environments and broader areas.

NU-Spidercam is more than an advanced field phenotyping tool. Due to its motion flexibility and sensor positioning/orientation accuracy, it can measure bidirectional reflectance distribution function of plant canopy, which is fundamental but notoriously difficult to measure in vegetation remote sensing. Combination of multispectral and thermal IR images along with the weather station data potentially allows inference of energy balance at the plot scale, and enables the calculation of evapotranspiration of different genetic lines to be tested. Finally, by varying agronomic inputs such as fertilizer or planting density, their relationships with plant growth, structural, and spectral characteristics can be rigorously quantified for various crops by NU-Spidercam. These are fundamental knowledge that have broad implications in agronomy and crop modeling research.

Acknowledgement

The funding for this work was provided by (1) University of Nebraska-Lincoln, (2) the Hatch Act capacity funding program (accession# 1011130) of USDA-NIFA, (3) National Science Foundation (DBI-1556186), (4) Nebraska Soybean Board, and (5) Nebraska Corn Board. The authors would like to thank Nathan Duffy for his long-hour assistance in the field to support the operation of NU-Spidercam; and graduate students Ali Mohammed, Shawn Jenkins, and Preston Hurst for collecting the ground truth data. Dr. Hector Santiago worked closely with the team to address many logistic challenges. Dr. Arthur I. Zygielbaum made the selection of the plant sensors mounted on NU-Spidercam. The authors would also like to thank the technical support team of Spidercam (Spidercam GmbH, Austria) working with us for this enjoyable and successful project.

Appendix A. Supplementary material

Supplementary data to this article can be found online at https://doi.org/10.1016/j.compag.2019.03.009.

References

Andrade-Sanchez, P., Gore, M., Heun, J., Thorp, K., Carmo-Silva, A., French, A., Salvucci, M., White, J., 2014. Development and evaluation of a field-based high throughput phenotyping platform. Funct. Plant Biol. 2014 (41), 68–79.

Araus, J.L., Cairns, J.E., 2013. Field high-throughput phenotyping: the new crop breeding frontier. Trends Plants Sci. 19, 52–61.

Bai, G., Ge, Y., Hussain, W., Baenziger, P.S., Graef, G., 2016. A multi-sensor system for high throughput field phenotyping in soybean and wheat breeding. Comput. Electron. Agric. 128, 181–192.

Furbank, R., Tester, M., 2011. Phenomics – technologies to relieve the phenotyping bottleneck. Trends Plant Sci. 16 (12), 635–644.

Gage, J.L., Jarquin, D., Romay, C., Lorenz, A., Buckler, E.S., Kaeppler, S., Alkhalifah, N., Bohn, M., Campbell, D.A., Edwards, J., Ertl, D., Flint-Garcia, S., Gardiner, J., Good, B., Hirsch, C.N., Holland, J., Hooker, D.C., Knoll, J., Kolkman, J., Kruger, G., Lauter, N., Lawrence-Dill, C.J., Lee, E., Lynch, J., Murray, S.C., Nelson, R., Petzoldt, J., Rocheford, T., Schnable, J., Schnable, P.S., Scully, B., Smith, M., Springer, N.M., Srinivasan, S., Walton, R., Weldekidan, T., Wisser, R.J., Xu, W., Yu, J., de Leon, N., 2017. The effect of artificial selection on phenotypic plasticity in maize. Nat. Commun. 8, 1348.

Ge, Y., Bai, G., Stoerger, V., Schnable, J.C., 2016. Temporal dynamics of maize plant growth, water use, and leaf water content using automated high throughput RGB and hyperspectral imaging. Comput. Electron. Agric. 127, 625–632.

Guanter, L., Zhang, Y., Jung, M., Joiner, J., Voigt, M., Berry, J.A., Frankenberg, C., Huete, A.R., Zarco-Tejada, P., Lee, J.-E., Moran, M.S., Ponce-Campos, G., Beer, C., Camps-Valls, G., Buchmann, N., Gianelle, D., Klumpp, K., Cescatti, A., Baker, J.M., Griffis, T.J., 2014. Global and time resolved monitoring of crop photosynthesis with chlorophyll fluorescence. PNAS 111 (14), E1327–E1333.

Irmak, S., Haman, D.Z., Bastug, R., 2000. Determination of crop water stress index for irrigation timing and yield estimation of corn. Agron. J. 92 (6), 1221–1227.

Jiang, Y., Li, C., Robertson, J.S., Sun, S., Xu, R., Paterson, A.H., 2018. GPhenoVision: a ground mobile system with multi-modal imaging for field-based high throughput phenotyping of cotton. Sci. Rep. 8, 1213.

Jimenez-Berni, J.A., Deery, D.M., Rozas-Larraondo, P., Condon, A., (Tony), G., Rebetzke, G.J., James, R.A., Bovill, W.D., Furbank, R.T., Sirault, X.R.R., 2018. High throughput determination of plant height, ground cover, and above-ground biomass in wheat with LiDAR. Front. Plant Sci. 9, 237.

Kirchgessner, N., Liebisch, F., Yu, K., Pfeifer, J., Friedli, M., Hund, A., Walter, A., 2017. The ETH field phenotyping platform FIP: a cable-suspended multi-sensor system. Funct. Plant Biol. 44, 154–168.

Li, L., Zhang, Q., Huang, D.F., 2014. A review of imaging techniques for plant phenotyping. Sensors 14 (11), 20078–20111.

Liang, Z., Pandey, P., Stoerger, V., Xu, Y., Qiu, Y., Ge, Y., Schnable, J., 2018. Conventional and hyperspectral time-series imaging for maize lines widely used in field trials. GigaScience 7, gix117.

Madec, S., Baret, F., de Solan, B., Thomas, S., Dutartre, D., Jezequel, S., Hemmerlé, M., Colombeau, G., Comar, A., 2017. High-throughput phenotyping of plant height: comparing unmanned aerial vehicles and ground LiDAR estimates. Front. Plant Sci. 8, 2002.

Meroni, M., Rossini, M., Gaunter, L., Alonson, L., Rascher, U., Colombo, R., Moreno, J., 2009. Remote sensing of solar-induced chlorophyll fluorescence: review of methods and applications. Remote Sens. Environ. 113, 2037–2051.

Pandey, P., Ge, Y., Stoerger, V., Schnable, J.C., 2017. High-throughput in vivo analysis of plant leaf chemical properties using hyperspectral imaging. Front. Plant Sci. 8, 1348.

Payero, J.O., Irmak, S., 2006. Variable upper and lower crop water stress index baselines for corn and soybean. Irrig. Sci. 25, 21–32.

Sankaran, S., Khot, L.R., Espinoza, C.Z., Jarolmasjed, S., Sathuvalli, V.R., Vandemark, G.J., Miklas, P.N., Carter, A.H., Pumphrey, M.O., Knowles, N.R., Pavek, M.J., 2015. Low-altitude, high-resolution aerial imaging systems for row and field crop phenotyping: a review. Eur. J. Agron. 70, 112–123.

Shi, Y., Thomasson, J.A., Murray, S.C., Pugh, N.A., Rooney, W.L., Shafian, S., Rajan, N., Rouze, G., Morgan, C.L.S., Neely, H.L., Rana, A., Bagavathiannan, M.V., Henrickson, J., Bowden, E., Valasek, J., Olsenholler, J., Bishop, M.P., Sheridan, R., Putman, E.B., Popescu, S., Burks, T., Cope, D., Ibrahim, A., McCutchen, B.F., Baltensperger, D.D., Avant Jr., R.V., Vidrine, M., Yang, C., 2016. Unmanned aerial vehicles for high-throughput phenotyping and agronomic research. PLoS ONE 11 (7), e0159781.

Sun, Y., Frankenberg, C., Wood, J.D., Schimel, D.S., Jung, M., Guanter, L., Drewry, D.T., Verma, M., Porcar-Castell, A., Griffis, T.J., Gu, L., Magney, T.S., Kohler, P., Evans, B., Yuen, K., 2017. OCO-2 advances photosynthesis observation from space via solar induced chlorophyll fluorescence. Science 358, eaam5747.

Underwood, J., Wendel, A., Schofield, B., McMurray, L., Kimber, R., 2017. Efficient in-field plant phenomics for row-crops with an autonomous ground vehicle. J. Field Rob. 34, 1061–1083.

Virlet, N., Sabermanesh, K., Sadeghi-Tehran, P., Hawkesford, M.J., 2017. Field Scanalyzer: an automated robotic field phenotyping platform for detailed crop monitoring. Funct. Plant Biol. 44, 143–153.

White, J.W., Andrade-Sanchez, P., Gore, M.A., Bronson, K.F., Coffelt, T.A., Conley, M.M., Kenneth, A., Feldmann, K.A., French, A.N., Heun, J.T., Hunsaker, D.J., Jenks, M.A., Kimball, B.A., Roth, R.L., Strand, R.J., Thorp, K.R., Wall, G.W., Wang, G.Y., 2012. Field-based phenomics for plant genetics research. Field Crops Res. 133, 101–122.

White, J.W., Conley, M.M., 2013. A flexible, low-cost cart for proximal sensing. Crop Sci. 53, 1646–1649.